# Anomalous Topological Active Matter

Kazuki Sone[1,*] and Yuto Ashida[1,2,†]
[1]Department of Applied Physics, The University of Tokyo, 7-3-1 Hongo, Bunkyo-ku, Tokyo 113-8656, Japan
[2]Department of Physics, University of Tokyo, 7-3-1 Hongo, Bunkyo-ku, Tokyo 113-0033, Japan

(Received 8 July 2019; published 12 November 2019)

Active systems exhibit spontaneous flows induced by self-propulsion of microscopic constituents and can reach a nonequilibrium steady state without an external drive. Constructing the analogy between the quantum anomalous Hall insulators and active matter with spontaneous flows, we show that topologically protected sound modes can arise in a steady-state active system in continuum space. We point out that the net vorticity of the steady-state flow, which acts as a counterpart of the gauge field in condensed-matter settings, must vanish under realistic conditions for active systems. The quantum anomalous Hall effect thus provides design principles for realizing topological metamaterials. We propose and analyze the concrete minimal model and numerically calculate its band structure and eigenvectors, demonstrating the emergence of nonzero bulk topological invariants with the corresponding edge sound modes. This new type of topological active systems can potentially expand possibilities for their experimental realizations and may have broad applications to practical active metamaterials. Possible realization of non-Hermitian topological phenomena in active systems is also discussed.

DOI: 10.1103/PhysRevLett.123.205502

*Introduction.*—Topologically nontrivial bands, which have been at the forefront of condensed matter physics [1–6], can also appear in various classical systems such as photonic [7–10] and phononic systems [11–17]. Such topologically nontrivial systems exhibit unidirectional modes that propagate along the edge of a sample and are immune to disorder. The existence of edge modes originates from the nontrivial topology characterized by bulk topological invariants of underlying photonic or acoustic band structures. The topological edge modes give rise to novel functionalities potentially applicable to, e.g., sonar detection and heat diodes [11,15]. Furthermore, they are argued to be closely related to the mechanism of robustness in biological systems [18,19].

On another front, active matter, a collection of self-driven particles, has attracted much interest as an ideal platform to study biological physics [20–22] and out-of-equilibrium statistical physics [23–28]. While a prototype of active matter has been originally introduced to understand animal flocking behavior [29,30], recent experimental developments have allowed one to manipulate and observe artificial active systems in a controlled manner by utilizing Janus particles [31], catalytic colloids [32], and external feedback control [33].

The aim of this Letter is to show that a topologically nontrivial feature can ubiquitously emerge in a nonequilibrium steady state of active matter and demonstrate it by analyzing the concrete minimal model, which can be realized with current experimental techniques. Specifically, we first point out that the net vorticity of the steady-state flow must vanish under realistic conditions for active systems in the continuum space. Since the vorticity in active matter can act as a counterpart of the magnetic field in condensed matter systems, this fact indicates that the quantum anomalous Hall effect (QAHE) naturally provides design principles for realizing topological metamaterials. We propose and analyze the active matter model inspired by the flat-band ferromagnet featuring the QAHE [34]. We numerically calculate its band structure and eigenvectors, and demonstrate that they exhibit nonzero topological invariants with the corresponding edge modes. Possible relation to non-Hermitian topological phenomena is also discussed.

Topological edge modes of active matter have been recently discussed by several authors [19,35–37]. There, the presence of nonzero net vorticity of the active flows, which can act as an effective magnetic field, was crucial to support topological edge modes reminiscent of the quantum Hall effect [1,38]. Yet, this required the introduction of rather intricate structures in active systems such as large defects [35], curved surface [36], and rotational forces [19,37]. One of the novel aspects introduced by this Letter is to eliminate these bottlenecks by constructing the analogy to the QAHE, significantly expanding possibilities for realizing topological metamaterials. Our proposal is based on the simplest setup on a flat continuum space with assuming no internal degrees of freedom (d.o.f.) of active particles. This class of systems is directly relevant to many realistic setups of active systems [39–43] and our design principle is applicable beyond the minimal model proposed here.

*Emergent effective Hamiltonian for active matter.*—To describe collective dynamics of active matter, we use the Toner-Tu equations [44–47], which are the hydrodynamic equations for active matter with a polar-type interaction:

 

$$\partial_t \rho + \nabla \cdot (\rho \mathbf{v}) = 0, \tag{1}$$

$$\begin{aligned}\partial_t \mathbf{v} + \lambda(\mathbf{v}\cdot\nabla)\mathbf{v} + \lambda_2(\nabla\cdot\mathbf{v})\mathbf{v} + \lambda_3\nabla|\mathbf{v}|^2 \\ = (\alpha - \beta|\mathbf{v}|^2)\mathbf{v} - \nabla P \\ + D_B\nabla(\nabla\cdot\mathbf{v}) + D_T\nabla^2\mathbf{v} + D_2(\mathbf{v}\cdot\nabla)^2\mathbf{v} + \mathbf{f},\end{aligned} \tag{2}$$

where $\rho(\mathbf{r}, t)$ is the density field of active matter and $\mathbf{v}(\mathbf{r}, t)$ is the local average of velocities of self-propelled particles. Equation (1) presents the equation of continuity. In Eq. (2), the first term of its right-hand side suggests a preference for a nonzero constant speed $|\mathbf{v}| = \sqrt{\alpha/\beta}$ if $\alpha$ is positive while negative $\alpha$ results in the nonordered state $|\mathbf{v}| = 0$. The coefficients in these equations can be obtained from microscopic models [48–53]. To simplify the problem, we ignore the terms including $\lambda_{2,3}$ and also the diffusive terms that contain the second-order derivative. This condition can be met in a variety of active systems [35,36,50]. Effects of $\lambda_{2,3}$ terms can be taken into account by renormalizing $\lambda$ if necessary [44]. We also assume that the pressure $P$ is proportional to $\rho$ as appropriate for an ideal gas.

Linearizing the Toner-Tu equations around a steady-state solution, we derive an eigenvalue equation for the fluctuations of density and velocity fields, $\delta\rho(\mathbf{r}, t) = \rho(\mathbf{r}, t) - \rho_{\rm ss}(\mathbf{r})$ and $\delta\mathbf{v}(\mathbf{r}, t) = \mathbf{v}(\mathbf{r}, t) - \mathbf{v}_{\rm ss}(\mathbf{r})$, respectively, where $\rho_{\rm ss}$ and $\mathbf{v}_{\rm ss}$ represent their steady-state values. We also assume that the steady-state speed $|\mathbf{v}_{\rm ss}|$ is much smaller than the sound velocity $c = \sqrt{P\rho_{\rm ss}/\rho}$. To clarify the argument, we define the following dimensionless variables: $\mathbf{r}' = \mathbf{r}/a$, $t' = ct/a$, $\delta\rho'(\mathbf{r}', t') = \delta\rho(a\mathbf{r}', at'/c)/\rho_{\rm ss}(a\mathbf{r}')$, $\delta\mathbf{v}'(\mathbf{r}', t') = \delta\mathbf{v}(a\mathbf{r}', at'/c)/c$, and $\mathbf{v}'_{\rm ss}(\mathbf{r}') = \mathbf{v}_{\rm ss}(a\mathbf{r}')/c$, where $a$ is a characteristic length of a system that we specify as a lattice constant later. For the sake of notational simplicity, hereafter we express the dimensionless variables $\mathbf{r}'$, $t'$, $\mathbf{v}'_{\rm ss}$ as $\mathbf{r}$, $t$, $\mathbf{v}_{\rm ss}$. The resulting linearized equation in the frequency domain is $\mathcal{H}\psi = \omega\psi$ with $\psi = (\delta\tilde{\rho}, \delta\tilde{v}_x, \delta\tilde{v}_y)^T$ and $\mathcal{H}$ being the effective Hamiltonian defined as

$$\mathcal{H} = \begin{pmatrix} -i\mathbf{v}_{\rm ss}\cdot\nabla & -i\partial_x & -i\partial_y \\ -i\partial_x & -i\lambda\mathbf{v}_{\rm ss}\cdot\nabla & 0 \\ -i\partial_y & 0 & -i\lambda\mathbf{v}_{\rm ss}\cdot\nabla \end{pmatrix}, \tag{3}$$

where $\delta\tilde{\rho}(\mathbf{r}, \omega)$, $\delta\tilde{v}_{x,y}(\mathbf{r}, \omega)$ are the Fourier components in the frequency domain. We here omit the spatial variation of $\rho_{\rm ss}$ and the divergence of $\mathbf{v}_{\rm ss}$ as justified in the Supplemental Material [54]. We note that, while the coefficient matrix $\mathcal{H}$ can be regarded as the effective Hamiltonian, it can in general be non-Hermitian when the diffusive terms in Eq. (2) are included.

*Absence of net vorticity in active matter.*—The linearized equation can be deformed into the Schrödinger-like equation [35]

$$(-i\nabla - \mathbf{V}_{\rm ss})^2\delta\tilde{\rho} = \omega^2\delta\tilde{\rho}, \tag{4}$$

where $\mathbf{V}_{\rm ss} = \omega(\lambda + 1)\mathbf{v}_{\rm ss}/2$ (see the Supplemental Material [54] for the derivation). Equation (4) demonstrates that $\mathbf{V}_{\rm ss}$ acts as the effective vector potential and its vorticity $\nabla \times \mathbf{V}_{\rm ss}$ can be interpreted as the effective magnetic field.

We consider active particles without internal d.o.f., which reside on a two-dimensional plane with a periodic structure of a unit cell $\Omega$. To avoid intricate structures, we assume that non-negligibly large defects are absent; i.e., the length of the perimeter of a defect in each unit cell can be neglected with respect to that of the unit-cell boundary $\partial\Omega$. We note that this condition does not preclude possibilities of minuscule defects created by, e.g., thin rods as realized in Ref. [43] or the presence of inhomogeneous potentials relevant to chemotactic bacteria subject to a nonuniform concentration of chemical compounds [55].

The net vorticity is then obtained by the integration over the unit cell and can be expressed via the Stokes' theorem as

$$\int_\Omega (\nabla \times \mathbf{V}_{\rm ss}) \cdot d\mathbf{S} = \oint_{\partial\Omega} \mathbf{V}_{\rm ss} \cdot d\mathbf{r}. \tag{5}$$

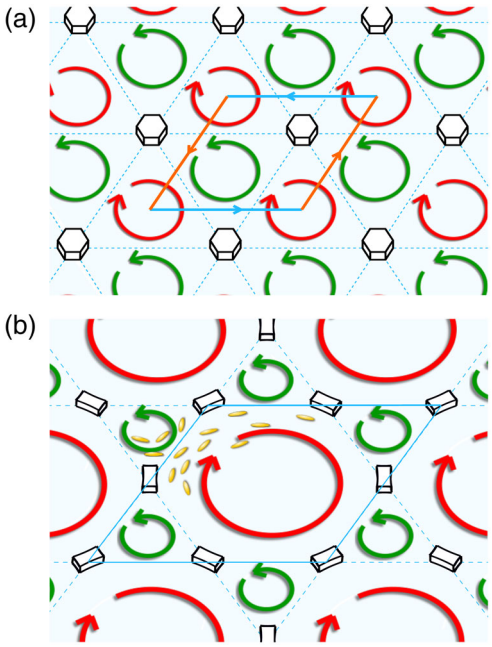


FIG. 1. Active particles on the two-dimensional flat space move under the influence of periodically aligned pillars. The red and green curved arrows represent the steady-state flows. (a) Triangular lattice geometry accompanying topologically trivial bands. The line integral along each boundary of the unit cell (blue and red solid lines) cancels each other because of the periodicity, leading to the vanishing net vorticity. (b) The proposed setup for topological active matter with kagome lattice geometry. Blue solid lines indicate the boundary of the unit cell. We set the side length of the unit cell as $a = 1$.

Because of a periodic structure of the steady flow along the unit-cell boundary $\partial\Omega$, one can show that the line integration on the right-hand side of Eq. (5) adds up to zero (see Fig. 1 for typical examples), resulting in the vanishing net vorticity. Thus, in the active hydrodynamics of interest here, it is prohibited to realize an analog of the quantum Hall effect, which requires an external magnetic field indicating nonzero net vorticity. Under the above conditions, we naturally arrive at the conclusion that a topological active matter must be realized as a counterpart of the QAHE, where the need for the external magnetic field can be mitigated.

We mention why the counterparts of the quantum Hall effect have been constructed in the previous setups [19,35–37] despite the above argument. The active particles in Refs. [19,37] exhibit self-rotations and thus their internal angular momenta violate our assumption on the absence of internal d.o.f. The model in Ref. [37] includes external rotational force, where the Coriolis force acts as an effective Lorentz force. In Ref. [35], the model includes large defects around which additional line integrals contribute to extra vorticity in Eq. (5). The curved space is discussed in Ref. [36]; it violates our assumption on flatness of the space. Altogether, these intricate structures allow one to realize the net effective magnetic field.

*The minimal model of topological active matter.*—To complete the analogy between the active matter and the QAHE, we propose the minimal model illustrated in Fig. 1(b). There, active particles obeying the Toner-Tu equations move under the influence of small pillars located at each site of a kagome lattice [56]. As illustrated in Fig. 1(b), the steady-state velocity field $\mathbf{v}_{\rm ss}(\mathbf{r})$ aligns on each boundary of triangular and hexagonal subcells separated by blue solid and dashed lines. Thus, particles in the triangular subcells circulate in the counterclockwise direction (green arrows) that is opposite to the direction of the particle circulation in the hexagonal subcells (red arrows) [57], resulting in the vanishing net vorticity. We confirm the emergence of this steady-state flow by performing the particle-based numerical simulation (see Supplemental Material [54] and movie).

It is noteworthy that such an "anticorrelated" velocity profile has been observed in bacterial experiments [43,58] and also in numerical simulations [35,59]. In the cases of triangular- and square-lattice structures [cf. Ref. [43] and Fig. 1(a)], however, only topologically trivial bands can appear due to the absence of a sublattice structure; this is why the kagome-lattice structure (as considered here) is crucial for realizing topological active matter.

*Topological band structure.*—We obtain the bulk dispersions by numerically diagonalizing the effective Hamiltonian $\mathcal{H}$. To obtain accurate results, we add the redundant d.o.f. without affecting the band structure by transforming $\mathcal{H}$ via a unitary matrix (see the Supplemental Material [54]). This transformation allows for calculations in the basis reflecting the centrosymmetry of the present system. Unless including this redundant d.o.f., one ends up with unphysical $k_y$-independent bands. While this prescription generates redundant eigenstates with eigenvalues of 0, it does not affect any physical properties including the topological feature. We thus analyze the eigenequation $\mathcal{H}'\psi' = \omega\psi'$ with $\psi' = (\delta\tilde{\rho}, \delta\tilde{v}_1, \delta\tilde{v}_2, \delta\tilde{v}_3)^T$ and $\mathcal{H}'$ being the effective Hamiltonian in the transformed frame

$$\mathcal{H}' = -i\begin{pmatrix} \mathbf{v}_{\rm ss}\cdot\nabla & \frac{2}{\sqrt{6}}\partial_1 & \frac{2}{\sqrt{6}}\partial_2 & \frac{2}{\sqrt{6}}\partial_3 \\ \frac{2}{\sqrt{6}}\partial_1 & \frac{2\lambda}{3}\mathbf{v}_{\rm ss}\cdot\nabla & -\frac{\lambda}{3}\mathbf{v}_{\rm ss}\cdot\nabla & -\frac{\lambda}{3}\mathbf{v}_{\rm ss}\cdot\nabla \\ \frac{2}{\sqrt{6}}\partial_2 & -\frac{\lambda}{3}\mathbf{v}_{\rm ss}\cdot\nabla & \frac{2\lambda}{3}\mathbf{v}_{\rm ss}\cdot\nabla & -\frac{\lambda}{3}\mathbf{v}_{\rm ss}\cdot\nabla \\ \frac{2}{\sqrt{6}}\partial_3 & -\frac{\lambda}{3}\mathbf{v}_{\rm ss}\cdot\nabla & -\frac{\lambda}{3}\mathbf{v}_{\rm ss}\cdot\nabla & \frac{2\lambda}{3}\mathbf{v}_{\rm ss}\cdot\nabla \end{pmatrix}, \quad (6)$$

where we define the variables as $\delta\tilde{v}_1 = 2\delta\tilde{v}_x/\sqrt{6} + \delta\tilde{v}_r/\sqrt{3}$, $\delta\tilde{v}_2 = -\delta\tilde{v}_x/\sqrt{6} + \delta\tilde{v}_y/\sqrt{2} + \delta\tilde{v}_r/\sqrt{3}$, and

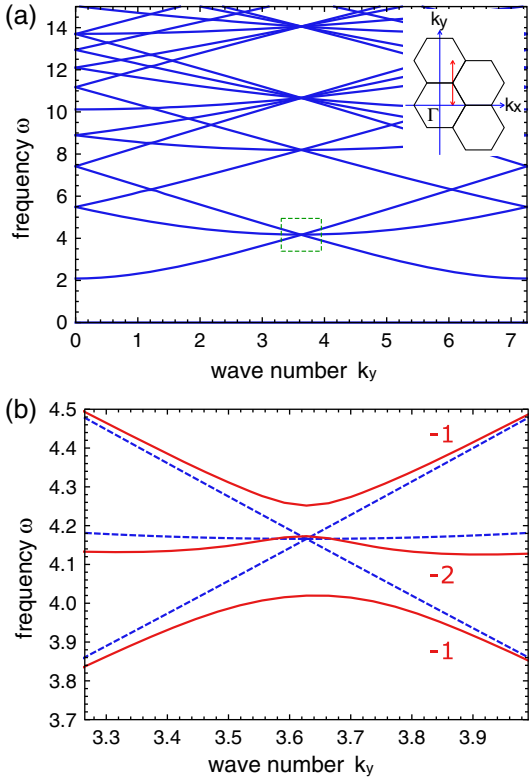


FIG. 2. (a) The band structure of the nonordered system, i.e., $\mathbf{v}_{\rm ss} = 0$. The dispersion is plotted along the line at $k_x = 2\pi/3$ with varying $k_y$ as indicated by the red arrow in the inset. We impose the twisted boundary conditions, $\psi(\mathbf{x}+\mathbf{a}) = e^{i\mathbf{k}\cdot\mathbf{a}}\psi(\mathbf{x})$, where $\psi$ is an eigenfunction and $\mathbf{a}$ is a lattice vector. The parameters used are $c = 1$, $\rho_{\rm ss} = 1$ and $\lambda = 0.8$. (b) The enlarged view of the band structure in the green dashed box in (a). The orange solid (blue dashed) curves show the results with (without) the steady-state flows. The integer number at each band represents the Chern number.

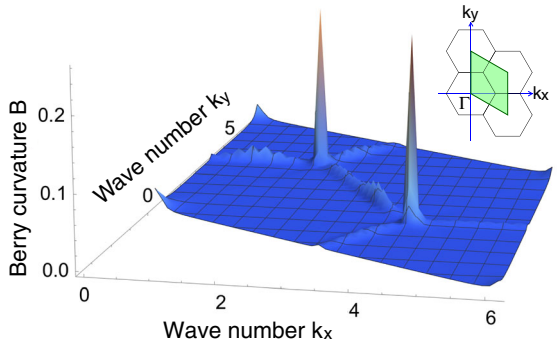


FIG. 3. Berry curvature of a topologically nontrivial band [the middle band with the Chern number $C = -2$ in Fig. 2(b)]. For the sake of visibility, the Berry curvature is plotted by inverting its sign. The parameters used are the same as in Fig. 2.

$\delta\tilde{v}_3 = -\delta\tilde{v}_x/\sqrt{6} - \delta\tilde{v}_y/\sqrt{2} + \delta\tilde{v}_r/\sqrt{3}$. Here, $\delta\tilde{v}_r$ is the redundant d.o.f. The derivatives denote $\partial_1 = \partial_x$, $\partial_2 = -\partial_x/2 + \sqrt{3}\partial_y/2$, and $\partial_3 = -\partial_x/2 - \sqrt{3}\partial_y/2$, which correspond to the directions along the grid lines of the kagome lattice [cf. the blue dashed and solid lines in Fig. 1(b)]. Figure 2 shows the band structure of the effective Hamiltonian $\mathcal{H}'$ calculated by the difference method [60]. Since the effective Hamiltonian satisfies the particle-hole symmetry, there is a counterpart for each eigenvector whose eigenenergy has the same absolute value and the opposite sign. For the nonordered case $|\mathbf{v}_{ss}| = 0$, there are degeneracies at the edges of the first Brillouin zone. Nonzero $|\mathbf{v}_{ss}|$ lifts those degeneracies and opens band gaps, characteristics of topological materials [3,7,9,10,12,15,16,34–36]. We note that our effective Hamiltonian does not contain nonderivative terms that are necessary for the original proposal of the QAHE [3]. The kagome-lattice structure mitigates this requirement [34] as it can realize the local flux without next-nearest hoppings.

We confirm that the proposed model exhibits a topologically nontrivial band by calculating the Chern number [2]. Specifically, the Chern number of the $n$th band is defined as

$$C_n = \frac{1}{2\pi}\int_{\mathrm{BZ}} \mathbf{B}_n(\mathbf{q}) \cdot d\mathbf{S}, \tag{7}$$

where $\mathbf{B}_n(\mathbf{q}) = \nabla_{\mathbf{q}} \times \mathbf{A}_n(\mathbf{q})$ is the Berry curvature with $\mathbf{A}_n(\mathbf{q}) = i\mathbf{u}_n(\mathbf{q}) \cdot [\nabla_{\mathbf{q}}\mathbf{u}_n(\mathbf{q})]$ being the Berry connection and $\mathbf{u}_n(\mathbf{q})$ being the $n$th eigenvector at wave number $\mathbf{q}$. We calculate the Berry curvature and the Chern number for each band following the numerical method proposed in Ref. [61]. The calculation shows that many of the bands have nonzero Chern numbers [see e.g., Fig. 2(b)]. Figure 3 shows an example of the Berry curvature of the topologically nontrivial acoustic band [cf. the middle band with $C = -2$ in Fig. 2(b)], which exhibits sharp peaks at the edges of the first Brillouin zone.

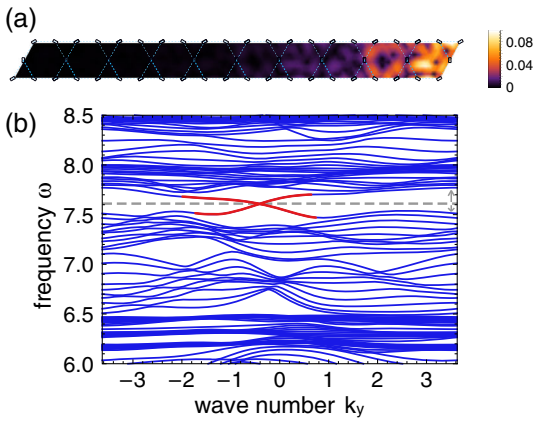


FIG. 4. (a) Spatial profile of the magnitude of the density fluctuation in an edge mode. The wave number and the frequency are set to be $k_y = -(4\sqrt{3}/15)\pi$ and $\omega = 7.6$, respectively. (b) The corresponding band structure under the open (periodic) boundary conditions in the $x$ ($y$) direction. The red curves show the dispersions associated with the edge mode in (a). The gray horizontal dashed line indicates the presence of the bulk band gap.

The bulk-edge correspondence predicts that the nonzero Chern number accompanies a unidirectional edge mode under open boundary conditions. While the correspondence has been well established in tight-binding lattice models, it has been recently argued to hold also in the continuum space [62]. To test the existence of edge modes, we calculate the sound modes for a supercell structure; 10 identical unit cells are aligned with open boundary conditions in the $x$ direction while the periodic boundary conditions are imposed in the $y$ direction. Figure 4 shows the band structure in this setup and the real-space profile of the sound mode at the gap between the topologically distinct bands. The density fluctuation rapidly decreases as we depart from the right end, indicating the presence of the edge mode [Fig. 4(a)]. The edge bands connect the lower and upper bulk bands [cf. the red curves in Fig. 4(b)]. There is one unidirectionally propagating mode for each edge at the bulk gap as consistent with the sum of the Chern numbers of the bands below the energy gap, $\sum_{n_<} C_{n_<} = -1$.

*Summary and Discussions.*—We showed that topologically nontrivial bands can arise in active systems without implementing intricate structures, which have been considered as prerequisites for realizing topological sound modes. Because of the vanishing net vorticity of steady-state flows, we pointed out that the quantum anomalous Hall effect provides a natural pathway to realize topological active materials. These findings are supported by numerical calculations of the band structure of the simple model, which is inspired by the flat-band ferromagnet in solid-state systems.

The present study opens several research directions. First, our results expand possibilities for experimental realizations of topological active systems. In particular,

the experimental setup realized by Ref. [43] is directly relevant to our model except for the lattice structure. Second, our work suggests a simple and general way to construct topological active matter by designing its periodic structure (steady-state flow) with making the analogy to a profile of a tight-binding lattice (gauge field) relevant to electronic topological materials.

Third, besides technological applications, one major motivation in the field of active matter is to advance our understanding of emergent nonequilibrium phenomena in biological systems. Biological systems modeled as active matter include, for example, cells, molecular motors, and cytoskeletons [30,47]. Topological edge modes may play an important role in various biological functionalities, which are often robust to disorder.

Finally, while we neglect the diffusive terms in the Toner-Tu equation (2), they can in general make the effective Hamiltonian non-Hermitian and suppress the high-wave-number modes. It is worthwhile to explore non-Hermitian topological phenomena in active systems; of particular interest is an exotic topological feature that has no counterpart in Hermitian systems [63–67]. In particular, asymmetrical flows in active matter may allow one to realize the non-Hermitian skin effect [65,66,68] and the quasiedge modes [67]. Such features could lead to an emergence of novel functionalities unique to active matter. We hope that our work stimulates further studies in these directions.

We thank Shunsuke Furukawa, Ryusuke Hamazaki, Takahiro Sagawa, Masahito Ueda, Daiki Nishiguchi, and Kazumasa Takeuchi for useful discussions. Y. A. acknowledges support from the Japan Society for the Promotion of Science through Program for Leading Graduate Schools (ALPS) and Grants No. JP16J03613 and No. JP19K23424.

*sone@noneq.t.u-tokyo.ac.jp
†ashida@ap.t.u-tokyo.ac.jp

[1] D. J. Thouless, M. Kohmoto, M. P. Nightingale, and M. den Nijs, Phys. Rev. Lett. **49**, 405 (1982).
[2] B. Simon, Phys. Rev. Lett. **51**, 2167 (1983).
[3] F. D. M. Haldane, Phys. Rev. Lett. **61**, 2015 (1988).
[4] C. L. Kane and E. J. Mele, Phys. Rev. Lett. **95**, 226801 (2005).
[5] M. Z. Hasan and C. L. Kane, Rev. Mod. Phys. **82**, 3045 (2010).
[6] X. L. Qi and S. C. Zhang, Rev. Mod. Phys. **83**, 1057 (2011).
[7] F. D. M. Haldane and S. Raghu, Phys. Rev. Lett. **100**, 013904 (2008).
[8] L. Lu, J. D. Joannopoulos, and M. Soljačić, Nat. Photonics **8**, 821 (2014).
[9] M. C. Rechtsman, J. M. Zeuner, Y. Plotnik, Y. Lumer, D. Podolsky, F. Dreisow, S. Nolte, M. Segev, and A. Szameit, Nature (London) **496**, 196 (2013).
[10] A. B. Khanikaev, S. Hossein Mousavi, W. K. Tse, M. Kargarian, A. H. MacDonald, and G. Shvets, Nat. Mater. **12**, 233 (2013).
[11] S. D. Huber, Nat. Phys. **12**, 621 (2016).
[12] L. M. Nash, D. Kleckner, A. Read, V. Vitelli, A. M. Turner, and W. T. M. Irvine, Proc. Natl. Acad. Sci. U.S.A. **112**, 14495 (2015).
[13] R. Süsstrunk and S. D. Huber, Science **349**, 47 (2015).
[14] C. L. Kane and T. C. Lubensky, Nat. Phys. **10**, 39 (2014).
[15] Z. Yang, F. Gao, X. Shi, X. Lin, Z. Gao, Y. Chong, and B. Zhang, Phys. Rev. Lett. **114**, 114301 (2015).
[16] R. Fleury, A. B. Khanikaev, and A. Alù, Nat. Commun. **7**, 11744 (2016).
[17] P. Delplace, J. B. Marston, and A. Venaille, Science **358**, 1075 (2017).
[18] A. Murugan and S. Vaikuntanathan, Nat. Commun. **8**, 13881 (2017).
[19] K. Dasbiswas, K. K. Mandadapu, and S. Vaikuntanathan, Proc. Natl. Acad. Sci. U.S.A. **115**, E9031 (2018).
[20] J. Brugués and D. Needleman, Proc. Natl. Acad. Sci. U.S.A. **111**, 18496 (2014).
[21] T. B. Saw, A. Doostmohammadi, V. Nier, L. Kocgozlu, S. Thampi, Y. Toyama, P. Marcq, C. T. Lim, J. M. Yeomans, and B. Ladoux, Nature (London) **544**, 212 (2017).
[22] K. Kawaguchi, R. Kageyama, and M. Sano, Nature (London) **545**, 327 (2017).
[23] C. Ganguly and D. Chaudhuri, Phys. Rev. E **88**, 032102 (2013).
[24] É. Fodor, C. Nardini, M. E. Cates, J. Tailleur, P. Visco, and F. van Wijland, Phys. Rev. Lett. **117**, 038103 (2016).
[25] S. Krishnamurthy, S. Ghosh, D. Chatterji, R. Ganapathy, and A. K. Sood, Nat. Phys. **12**, 1134 (2016).
[26] D. Mandal, K. Klymko, and M. R. DeWeese, Phys. Rev. Lett. **119**, 258001 (2017).
[27] P. Pietzonka and U. Seifert, J. Phys. A, **51**, 01LT01 (2017)
[28] D. Martin, C. Nardini, M. E. Cates, and É. Fodor, Europhys. Lett. **121**, 60005 (2018).
[29] T. Vicsek, A. Czirók, E. Ben-Jacob, I. Cohen, and O. Shochet, Phys. Rev. Lett. **75**, 1226 (1995).
[30] T. Vicsek and A. Zafeiris, Phys. Rep. **517**, 71 (2012).
[31] H. R. Jiang, N. Yoshinaga, and M. Sano, Phys. Rev. Lett. **105**, 268302 (2010).
[32] J. Palacci, S. Sacanna, A. P. Steinberg, D. J. Pine, and P. M. Chaikin, Science **339**, 936 (2013).
[33] U. Khadka, V. Holubec, H. Yang, and F. Cichos, Nat. Commun. **9**, 3864 (2018).
[34] K. Ohgushi, S. Murakami, and N. Nagaosa, Phys. Rev. B **62**, R6065 (2000).
[35] A. Souslov, B. C. Van Zuiden, D. Bartolo, and V. Vitelli, Nat. Phys. **13**, 1091 (2017).
[36] S. Shankar, M. J. Bowick, and M. C. Marchetti, Phys. Rev. X **7**, 031039 (2017).
[37] A. Souslov, K. Dasbiswas, M. Fruchart, S. Vaikuntanathan, and V. Vitelli, Phys. Rev. Lett. **122**, 128001 (2019).
[38] K. v. Klitzing, G. Dorda, and M. Pepper, Phys. Rev. Lett. **45**, 494 (1980).
[39] A. Sokolov, I. S. Aranson, J. O. Kessler, and R. E. Goldstein, Phys. Rev. Lett. **98**, 158102 (2007).
[40] A. Cavagna, A. Cimarelli, I. Giardina, G. Parisi, R. Santagati, F. Stefanini, and M. Viale, Proc. Natl. Acad. Sci. U.S.A. **107**, 11865 (2010).

[41] J. Deseigne, O. Dauchot, and H. Chaté, Phys. Rev. Lett. **105**, 098001 (2010).
[42] V. Schaller, C. Weber, C. Semmrich, E. Frey, and A. R. Bausch, Nature (London) **467**, 73 (2010).
[43] D. Nishiguchi, I. S. Aranson, A. Snezhko, and A. Sokolov, Nat. Commun. **9**, 4486 (2018).
[44] J. Toner and Y. Tu, Phys. Rev. Lett. **75**, 4326 (1995).
[45] J. Toner and Y. Tu, Phys. Rev. E **58**, 4828 (1998).
[46] J. Toner, Y. Tu, and S. Ramaswamy, Ann. Phys. (Amsterdam) **318**, 170 (2005).
[47] M. C. Marchetti, J. F. Joanny, S. Ramaswamy, T. B. Liverpool, J. Prost, M. Rao, and R. A. Simha, Rev. Mod. Phys. **85**, 1143 (2013).
[48] E. Bertin, M. Droz, and G. Grégoire, Phys. Rev. E **74**, 022101 (2006).
[49] A. Peshkov, E. Bertin, F.Ginelli, and H. Chaté, Eur. Phys. J. Spec. Top. **223**, 1315 (2014).
[50] F. D. C. Farrell, M. C. Marchetti, D. Marenduzzo, and J. Tailleur, Phys. Rev. Lett. **108**, 248101 (2012).
[51] A. P. Solon and J. Tailleur, Phys. Rev. Lett. **111**, 078101 (2013).
[52] R. Suzuki, C. A. Weber, E. Frey, and A. R. Bausch, Nat. Phys. **11**, 839 (2015).
[53] A. Bricard, J. B. Caussin, N. Desreumaux, O. Dauchot, and D. Bartolo, Nature (London) **503**, 95 (2013).
[54] See Supplemental Material at http://link.aps.org/supplemental/10.1103/PhysRevLett.123.205502 for the detailed discussions and the additional numerical results.
[55] J. Saragosti, V. Calvez, N. Bournaveas, B. Perthame, A. Buguin, and P. Silberzan, Proc. Natl. Acad. Sci. U.S.A. **108**, 16235 (2011).
[56] We assume that, while these pillars can influence the flow of particles, their sizes are small enough such that the conditions discussed above Eq. (5) are satisfied.
[57] The reversed flow $-\mathbf{v}_{ss}$ is also allowed as a steady-state solution; the initial condition determines which flow can be realized in a system.
[58] H. Wioland, F. G. Woodhouse, J. Dunkel, and R. E. Goldstein, Nat. Phys. **12**, 341 (2016).
[59] D. J. Pearce and M. S. Turner, J. R. Soc. Interface **12**, 20150520 (2015).
[60] G. D. Smith, *Numerical Solution of Partial Differential Equations: Finite Difference Methods* (Oxford University Press, Oxford, UK, 1985).
[61] T. Fukui, Y. Hatsugai, and H. Suzuki, J. Phys. Soc. Jpn. **74**, 1674 (2005).
[62] M. G. Silveirinha, Phys. Rev. X **9**, 011037 (2019).
[63] T. E. Lee, Phys. Rev. Lett. **116**, 133903 (2016).
[64] D. Leykam, K. Y. Bliokh, C. Huang, Y. D. Chong, and F. Nori, Phys. Rev. Lett. **118**, 040401 (2017).
[65] F. K. Kunst, E. Edvardsson, J. C. Budich, and E. J. Bergholtz, Phys. Rev. Lett. **121**, 026808 (2018).
[66] S. Yao and Z. Wang, Phys. Rev. Lett. **121**, 086803 (2018).
[67] Z. Gong, Y. Ashida, K. Kawabata, K. Takasan, S. Higashikawa, and M. Ueda, Phys. Rev. X **8**, 031079 (2018).
[68] S. Longhi, Phys. Rev. Res. **1**, 023013 (2019).